Published in final edited form as:
*Vis Neurosci*. 2007 ; 24(1): 111–123. doi:10.1017/S0952523807070149.

# Generation, Identification and Functional Characterization of the *nob4* Mutation of *Grm6* in the Mouse

**Lawrence H. Pinto**[1], **Martha H. Vitaterna**[1], **Kazuhiro Shimomura**[1], **Sandra M. Siepka**[1], **Erin L. McDearmon**[1,4], **Victoria Balannik**[1], **Chiaki Omura**[1], **Stephen Lumayag**[1], **Brandon M. Invergo**[1], **Brett Glawe**[1], **Donald R. Cantrell**[2], **Samsoon Inayat**[2,10], **Marissa A. Olvera**[3], **Kirstan A. Vessey**[5], **Maureen A. McCall**[5,6], **Dennis Maddox**[7], **Catherine W. Morgans**[8], **Brandon Young**[9], **Mathew T. Pletcher**[9], **Robert F. Mullins**[3], **John B. Troy**[2], and **Joseph S. Takahashi**[1,4]

[1]Department of Neurobiology and Physiology and Center for Functional Genomics, Northwestern University, Evanston, IL 60208

[2]Department of Biomedical Engineering McCormick School of Engineering, Northwestern University, Evanston, IL 60208

[3]Department of Ophthalmology & Visual Sciences, University of Iowa, Iowa City, IA52242

[4]Howard Hughes Medical Institute

[5]Department of Psychological and Brain Sciences University of Louisville, Louisville, KY

[6]Department of Ophthalmology & Visual Sciences, University of Louisville, Louisville, KY

[7]The Jackson Laboratory, Bar Harbor, ME

[8]Neurological Sciences Institute, Oregon Health and Science University, Beaverton, OR

[9]The Scripps Research Institute, Jupiter, FL

[10]Department of Mechatronics and Control Engineering, University of Engineering and Technology, Lahore, Pakistan

## Abstract

We performed genome-wide chemical mutagenesis of C57BL/6J mice using *N*-ethyl-*N*nitrosourea (ENU). Electroretinographic screening of the third generation offspring revealed two G3 individuals from one G1 family with a normal a-wave but lacking the b-wave that we named *nob4*. Th e mutation was transmitted with a recessive mode of inheritance and mapped to chromosome 11 in a region containing the *Grm6* gene, which encodes a metabotropic glutamate receptor protein, mGluR6. Sequencing confirmed a single nucleotide substitution from T to C in the *Grm6* gene. The mutation is predicted to result in substitution of Pro for Ser at position 165 within the extracellular, ligand-binding domain and oocytes expressing the homologous mutation in mGluR6 did not display robust glutamate-induced currents. Retinal mRNA levels for *Grm6* were not significantly reduced, but no immunoreactivity for mGluR6 protein was found. Histological and fundus evaluations of *nob 4* showed normal retinal morphology. In contrast, the mutation has severe consequences for visual function. In *nob4* mice, fewer retinal ganglion cells (RGCs) responded to the onset (ON) of a bright full field stimulus. When ON responses could be evoked, their onset was significantly delayed. Visual acuity and contrast sensitivity, measured with optomotor responses, were reduced under both photopic and scotopic conditions. This mutant will

Please address editorial correspondence to: Lawrence H. Pinto, Ph.D. Northwestern University, Dept. Neurobiology & Physiology 2205 Tech Dr. Northwestern University, Evanston, IL 60208, Voice: 847-491-7915, Fax: 847-491-5211, larry-pinto@northwestern.edu.

be useful because its phenotype is similar to that of human patients with congenital stationary night blindness and will provide a tool for understanding both retinal circuitry and the role of ganglion cell encoding of visual information.

### Keywords

Chemical mutagenesis; forward genetics; retina; retinal ganglion cells; depolarizing bipolar cells; congenital stationary night blindness; ON pathway; molecular cloning; positional cloning; gene discovery; rod pathway; visual acuity

## Introduction

One of the most notable features of the visual system is the division of signals into parallel pathways, initiated at the synapse between photoreceptors and the second order bipolar cells. This parallel organization is maintained through higher levels of the retinorecipient nuclei of the brain. Ever since Kuffler's (Kuffler, 1953) description of ON-and OFF-center retinal ganglion cells (RGCs), the physiological and biochemical mechanisms for the ON and OFF parallel pathways have been under investigation. Of particular note was the discovery that a metabotropic glutamate receptor, mGluR6 (Masu *et al.*, 1995), was responsible for initiating the ON pathway (Slaughter & Miller, 1981). Using an intracellular, second messenger-mediated cascade, mGluR6 creates a sign-inverting depolarization in ON bipolar cells from the hyperpolarization of illuminated photoreceptors. Elimination of the *Grm6* gene encoding this receptor, using gene targeting, results in an elimination of RGC responses to onset of a bright stimulus (ON responses) (Masu *et al.*, 1995; Renteria *et al.*, 2006).

Gene knockouts are useful in defining the functional role of a particular protein in a given system. However, a genetic analysis of a complex process, such as initiation of the mGluR6 mediated cascade, can be better served by an allelic series of mutations that permit a detailed dissection of the underlying biochemical mechanisms. To this end, we have performed a search for random, chemically-induced mutations that affect the electroretinogram (ERG) (Pinto *et al.*, 2004). Our search has yielded several mutants (Vitaterna *et al.*, 2006), and among them one showed a normal a-wave but lacked the b-wave of the ERG. Further, the retina in these mutants had normal morphology. Since this was the fourth mouse mutation that produced this phenotype, we named this new mutant *nob4*. Among the others are *nob* (Pardue *et al.*, 1998), a mutation in the *nyx* gene that encodes the nyctalopin protein and *nob2* (Chang *et al.*, 2006), a mutation in the *Cacna1f* gene that encodes the α1F subunit of the voltage dependent calcium channel, responsible for glutamate release from photoreceptors.

Because we took a forward genetics approach, the *nob4*gene's identity was unknown. Thus, a genetic approach was needed to map the gene and to identify the underlying mutation. Our experiments led to the identification of a point mutation in the coding region of *Grm6*. The effects of the *nob4*mutation on retina l structure and function were consistent with results recently observed in *mGluR6* knockout mice. In both mice, retinal morphology was normal, but the absence of mGluR6 expression produced significant deficits in visually-evoked responses of RGCs. In addition, we characterized the visually-guided behavior of *nob4*mice and found severe deficits in spatial vision. Since *nob4* results from a point mutation in the ligand binding portion of the mGluR6 protein, this mouse model should be useful for understanding the contribution of the ON pathway to visually-guided behaviors, dissecting the retinal circuitry of the ON pathway and defining biochemical mechanisms of bipolar cell signal generation.

## Methods

For all experiments described mice were treated in accordance with the Animal Care and Use Committees at each of the institutions and in compliance with the American Physiological Society and Society for Neuroscience statements for ethical care and use of animals.

### Mutagenesis and mouse production

Details of the mutagenesis and screening procedures have been published previously (Pinto *et al.*, 2005). Male C57BL/6J mice were mutagenized with three, weekly doses of *N-nitroso-N-ethylurea* (90–100 mg/kg body weight) starting at 6 weeks of age. ENU treated males were bred with WT females to produce mutant generation 1 (G1) offspring, in which each mouse represents one mutagenized gamete. G1 males and G1 females from *different* G0 founders were intercrossed with one another to produce G2 mice, and G2 siblings were then intercrossed (as breeding trios when possible) to generate G3 offspring for phenotyping. Sufficient breeding pairs were used to give a >80% probability of detecting a recessive mutation in the kindred; six G2 intercrosses were established for each kindred and at least six G3 pups tested per G2 mother (Siepka & Takahashi, 2005). All G3 mice were screened for a number of neurobiological traits starting at 6 weeks of age (Vitaterna *et al.*, 2006) and were tested for the electroretinogram starting at 12 weeks of age.

### Electroretinogram

Scotopic ERGs were performed in total darkness with the aid of infrared image converters (Rigel Optics) and infra-red safelamps (Kodak, #11 filter) as described previously (Pinto *et al.*, 2005). Mice were dark-adapted for at least 2 hours prior to recording. Anesthesia was induced with a mixture of ketamine (70 mg/kg) and xylazine (7 mg/kg) administered intraperitoneally and body temperature was maintained between 36.5–37 °C. ERGs were obtained by differential recording of the corneal voltages between the two eyes with Dawson, Trick, and Litzkow (DTL) silver/nylon fiber electrodes (Dawson *et al.*, 1979). The corneas were wetted with a solution of 1.2% cellulose in 0.9% NaCl. Diffuse stimuli were presented from LEDs to the right eye which was covered with a clear contact lens made from heat-molded plastic film (Aclar®). The left eye was covered with an opaque contact lens. Nine full-field flash stimuli (luminance $7\times10^{-4}$ to 300 cd·sec/$m^2$) were presented against a dark background for the scotopic ERG. Subsequently, a steady, dim adapting light (0.5 cd/$m^2$) was presented steadily in order to saturate the rod contribution. The adapting light was presented during the 15 sec interval when a flash stimulus (luminance 0.2 cd·sec/$m^2$) was applied repetitively in order to evoke the photopic ERG. The ERG was recorded at 1kHz with a resolution of 0.5 μV. Response averaging was employed for the responses to dim stimuli to increase their signal-to-noise ratio. Responses were filtered to remove oscillatory potentials that occur at about the time of the peak of the b-wave of the electroretinogram. All stimulus presentation and data recording were controlled by software that is available to the scientific community (http://www.neuromice.org/browseAssays.do, or http://www.genome.northwestern.edu/neuro/vision_protocol.cfm). Analysis of the ERGs was done automatically using MATLAB analysis software (the Mathworks, Inc.). The peak amplitude of the a-, b-and c-waves of the ERG was assessed under scotopic and photopic conditions. For very dim stimuli, the amplitude of the scotopic threshold response (STR), which is an indicator of post-photoreceptor, inner retinal activity (Saszik *et al.*, 2002) was also assessed.

### Fundus photography

The iris was dilated with 1% tropicamide (Mydriacil®), the corneas kept moist with saline solution, and body temperature maintained between 36.5–37 °C during photography. Digital

images were made with a small animal fundus camera (model KD-211C, Kowa, Tokyo, Japan, 2.5 megapixels) equipped with a 66 diopter supplemental lens.

## Genotyping

All of the genotyping was accomplished by use of a single-base extension reaction using the Sequenom genotyping platform. This is a two step process. First, the region containing the SNP is amplified. Then, a primer ending at the polymorphic site is used for the single-base extension reaction. The products are then sorted by matrix-assisted laser desorption ionization, time-of-flight mass spectrometry (MALDI-TOF MS). Briefly, primers for PCR and single base extension reactions were designed by using the MassARRAY Assay Design 3.0 software package (Sequenom, Inc., San Diego, CA). 1ml of 2.5–10ng/ml genomic DNA was combined with 1.85ml of water, 0.1ml of 25 mM dNTPs (Invitrogen Corp., Carlsbad, CA), 0.1ml of 5 units/ml HotStar *Taq* (Qiagen Inc., Valencia CA), 0.625ml of 10x HotStar PCR buffer containing 15 mM MgCl2, 1ml PCR primers mixed together at a concentration of 500nM for multiplexed reactions, and 0.325ml of 25 mM MgCl2. Reactions were heated at 95°C for 15 min followed by 45 cycles at 95°C for 20 s, 56°C for 30 s, and 72°C for 1 min and a final incubation at 72°C for 3 min. After PCR amplification, remaining dNTPs were dephosphorylated by adding 1.5ml of water, 0.17ml of 10x SAP buffer (Sequenom, Inc., San Diego, CA), and 0.3 units of shrimp alkaline phosphatase (Sequenom, Inc., San Diego, CA). The reaction was placed at 37°C for 20 min, and the enzyme was deactivated by incubating at 85°C for 5 min. After shrimp alkaline phosphatase treatment, the genotyping reaction was combined with 0.76ml of water, 0.2ml of iPLEX termination mix (Sequenom, Inc., San Diego, CA), 0.04ml of iPLEX Enzyme (Sequenom, Inc., San Diego, CA), 0.2ml of 10x iPLEX Buffer, and 0.81ml of 7 to 14mM multiplexed extension primers. The MassEXTEND reaction was carried out at 94°C for 2 min and then 99 cycles of 94°C for 5 s, 52°C for 5 s, and 72°C for 5 s. The reaction mix was desalted by adding 3 mg of a cationic resin, SpectroCLEAN (Sequenom, Inc., San Diego, CA), and resuspended in 30ml of water. Completed genotyping reactions were spotted in nanoliter volumes onto a matrix arrayed into 384 elements on a silicon chip (Sequenom SpectroCHIP), and the allele-specific mass of the extension products were determined by MALDI-TOF MS. Analysis of data was accomplished using the SPECTROTYPER software.

Initially, eight mice (six mutant and two WT littermates) were typed with a panel of 303 SNP assays evenly spaced across the genome. A 40Mb region on MMU11 showed a perfect phenotype-genotype correlation. The eight original samples and an additional 31 were genotyped at a higher marker density in this region, narrowing the candidate region to 28Mb on MMU11, between 29Mb and 57Mb.

## Grm6 messenger RNA abundance

Gene expression assays were performed as previously described (Pinto *et al.*, 2005). Briefly, total RNA was extracted from mouse retinas (four retinas from 2 mice of each genotype) using Trizol (Invitrogen, San Diego, CA), according to manufacturer's instructions. RNA concentration was measured by spectrophotometry and samples were normalized by diluting in DEPC-treated sterile water. TaqMan real-time (quantitative) PCR assays were performed using the comparative CT method, with an ABI 7700 Sequence Detector and TaqMan EZ RT-PCR kit reagents (ABI, Foster City, CA). Control probe and primer sets have been described previously (Pinto *et al.*, 2005). The probe for *Grm6* was 5'CCGCTTCAATGGTGACGCAGGAAC3' and the *mGrm6* primers were F: 5'CGGACCCTGCTGCACTACAT3' and R: 5'CCCCATTCTCATTGAACATCACT3'.

### Immunohistochemistry and Microscopy

Mouse retinal sections were prepared and stained as described previously (Morgans *et al.*, 2005). Antibodies were used at the following concentrations: mGluR6 (Morgans *et al.*, 2006), 1:100; PKCα (Sigma, St Louis, MO), 1:5000. Appropriate secondary antibodies were coupled to either CY3 (Jackson Immunochemicals, West Grove, PA) and diluted 1:500, or Alexa-488 (Molecular Probes, Eugene, OR) and diluted 1:1000. Images were acquired on a Zeiss LSM 510 confocal microscope with a 63x/1.40 oil immersion objective. All figures shown are projections of several consecutive optical sections of <1μm thickness each for a total thickness of 3–5μm. For figures, brightness and contrast of images were optimized with Adobe Photoshop 7.0.

### Molecular Biology and in-vitro cRNA transcription

The cDNA of mGluR2 (a gift of Dr. J. P. Pin) was cloned into the pBlueScript SK⁻vector, the cDNA of mGluR6 (a gift of Dr. D. Hampson) and the cDNA of Gαo-1were cloned into the pGEM-HJ vector, and the cDNAs of GIRK1 and GIRK2 were cloned into the pBS-MXT vector (gifts from Dr. N. Dascal). Point mutations in mGluR2 and mGluR6 were created by PCR using the QuikChange method (Stratagene, La Jolla, CA) and verified by double-strand DNA sequencing. Numbering of amino acids starts from the first methionine of the ORF. For expression in oocytes, plasmids were linearized with *NotI* (mGluR2, mGluR6 and Gαo-1) or with *SalI* (GIRK1 and GIRK2). Capped cRNA was transcribed *in vitro* using T3 or T7 RNA polymerases as appropriate (mMessage mMachine; Ambion, Austin, TX).

### Heterologous expression and electrophysiological recordings

Stage V-VI *Xenopus laevis* oocytes were prepared as described previously (Shimbo *et al.*, 1996). Oocytes were either injected with 0.2 ng of GIRK1 and GIRK2 cRNAs and 10ng of mGluR2 cRNA or were injected with 0.2 ng of GIRK1 and GIRK2 cRNAs, 1ng of Gαo-1 and 10ng of mGluR6 cRNAs at 50 nl/oocyte, and assayed 3 days later. Two electrode voltage clamp recordings were carried out using TEV-200 (Dagan, Minneapolis, MN) connected to DIGIDATA 1440A and pCLAMP10 (Axon Instruments, Foster City, CA). Oocyte perfusion and agonist application have been described previously (Sharon *et al.*, 1997). Currents were recorded at a holding potential of −80 mV. Recorded oocytes were homogenized in lysis buffer (50mM Tris-HCl pH 8.0, 150mM NaCl, 1% Triton X-100 in the presence of a cocktail of protease inhibitors (Cǿmplete; Roche Diagnostics GmbH, Germany)). Western blot analysis was performed as described previously (Stern-Bach *et al.*, 1994). Primary antibodies anti-rat mGluR2 and anti-mGluR6 (Abcam, Cambridge, MA) were used at 1:500 dilution.

### In vitro recordings of mouse retinal ganglion cell responses

Mice were euthanized by cervical dislocation. Their eyes were enucleated under dim red illumination and placed into a Petri dish containing an Artificial Cerebrospinal Fluid (ACSF) with the following composition (mM): NaCl, 124; KCl, 2.5; CaCl2, 2; MgCl2, 2; NaH2PO4, 1.25; Glucose, 22; NaHCO3, 26; and HEPES 20 (pH 7.35–7.45). Isolation of the retina was performed in ACSF under infrared illumination using a microscope equipped with infrared converters. The eyes were punctured at the ora serata with a sharp blade, and this incision was extended around the full circumference of the eye with a small pair of scissors. The anterior portion of the eye, along with the lens and much of the vitreous, was gently separated from the posterior portion of the eye, and the remaining vitreous was removed with a pair of forceps. Beginning at the periphery and moving toward the optic nerve, the sclera was gently teased away from the retina. Finally, the optic nerve and the attached sclera were cut from the retina to complete the dissection. The retina, placed ganglion cell side up on a nitrocellulose filter paper, was placed onto the microelectrode

array (Multichannel Sysems Darmstadt, Germany) and secured with a small manipulator. The array chamber (0.5 ml) was placed in the preamplifier on an inverted microscope stage. The retina was superfused with oxygenated (95% O2, 5% CO2) ACSF maintained at 34°C with a 2ml/min flow rate. The retina was allowed to stabilize for at least one hour before recordings were begun. This entire procedure, from animal sacrifice to superfusion with ACSF needed to be performed in 15 to 20 minutes for reliable recordings to be made.

A uniform field was projected onto the retina through the objective lens of the microscope using one of its light input ports. The stimulus was generated on a Sony Multiscan 17se monitor running at a frame rate of 150 Hz and controlled by a video card and software interface (VSG, Cambridge Research Systems). The stimulus consisted of a 1s Light-ON period followed by a 1s Light-OFF period whose luminance at the retina was 3 cd/$m^2$ during the light-ON period.

Voltage signals from the microelectrodes were amplified by the MCS preamplifier (bandpass 1–5000 Hz) and recorded using MCRack software. Noise did not exceed ±20 μV. Signals were high-pass filtered digitally at 25 Hz, and spikes were detected with a –51 μV threshold. Spike sorting was performed in Offline Sorter (Plexon Inc.) using an automated 2D T-Distribution Expectation Minimization algorithm. Spike timestamps were exported to MATLAB where custom scripts were used for further data analysis.

Peristimulus time histograms (PSTHs) and raster plots of individual units were generated. Upon visual inspection, units without a visual response were identified and categorized as NONRESPONSIVE. Visually responsive units lacking clear peaks at either stimulus onset (ON) or offset (OFF) portions of the stimulus were categorized as OTHER. The remaining units were classified as either ON, OFF, or ON-OFF based on the ratio of mean spike rates during the ON portion (RON) and OFF portions (ROFF) of the full field stimulus. Cells with RON/ ROFF ratios great than 4 were classified as ON cells, those with ratios less than 0.25 were classified as OFF cells, and the remaining were classified as ONOFF cells (Nirenberg & Meister, 1997; Nirenberg *et al.*, 2001), but see (Sagdullaev & McCall, 2005)).

To provide a quantitative measure of the time-course of high spike activity, histograms were generated by counting, for every cell, the times of the PSTH bins with firing rates greater than one standard deviation above the mean firing rate of the cell (high spike activity). Additionally, to analyse the latency of the ON and OFF responses, PSTHs were smoothed using a Gaussian kernel ($\sigma$ = 25 ms), and the time to maximum peak was determined for both the ON and OFF segments of the light stimulus. For ON responses, the latency measures the time from onset of the light stimulus, and, for OFF responses, the latency measures time from offset of the light stimulus

### In vivo recordings of mouse RGC responses

RGCs were recorded from *nob4* (n=4) and WT mice (n=6) aged 35–60 days. Surgical techniques, as well as visual stimulation and recording protocols, have been published previously (Sagdullaev & McCall, 2005; Chang *et al.*, 2006). Anesthesia was induced, as described above for the ERG assessments and the mouse was mounted in a stereotaxic frame. A small craniotomy was performed and the cortex was removed by vacuum suction to visualize the optic nerve. Eyedrops (1% mydriacyl, 2.5% phenylephrine HCl) were used to dilate the pupil and to paralyze accommodation. A tungsten electrode (40–70 MQ impedance) was inserted into the optic nerve anterior to the chiasm and action potentials from individual retinal ganglion cell (RGC) axons were amplified and digitized at 15 kHz. RGC responses were played in real time over an audiomonitor and displayed on both an oscilloscope and a computer monitor, and stored for offline analysis, using Spike2 software. The receptive field (RF) of each isolated RGC was mapped onto a tangent screen (placed 25

cm from the nodal point of the mouse's eye), using a handheld Pantoscope or flashlight. The tangent screen was replaced with a computer display monitor centered on the RF and located at the same distance. Computer controlled visual stimuli were presented on the monitor using Vision Works for Electrophysiology software. RGCs were adapted to a full field luminance 75 cd/m$^2$ for three minutes and then stimulated with a full field flashes for 5 s ON (150 cd/m$^2$) and 5 s OFF (0 cd/m$^2$) for a total of 30 cycles.

Responses were collected and displayed as both averaged PSTHs (50 ms bin width) and individual raster plots. For analysis of response characteristics, averaged PSTHs were smoothed over a 100 ms bin width to a raised cosine function and a significant response was defined as a response to stimulus onset (ON) or offset (OFF) whose peak was above the mean firing rate at 75 cd/m$^2$ + three SEM. Peak firing rate and time to peak (TTP) after the stimulus onset also were determined from the smoothed PSTH.

### Optomotor responses

Spatial acuity and contrast threshold of awake, unrestrained mice were assessed under both scotopic and photopic conditions using the OptoMotry device (Cerebral Mechanics, Lethbridge, AL). Head movements in response to a rotating sinusoidally-modulated grating were scored as previously described (Pinto *et al.*, 2005) by an observer who was neither able to observe the direction of movement of the stimuli nor aware of the genotype of the mouse. The use of the simple staircase protocol allowed the observer to focus attention to the movements of the mouse's head (McGill *et al.*, 2004). Behavioral measurements were made between 1300h and 1600h. In order to test at low light levels, large neutral density filters were applied directly to the surfaces of the liquid crystal displays. In order to view the mouse at low light levels a camera that is sensitive to infrared illumination (Fire-i board camera, Unibrain, San Ramon, CA 94583) and two infrared light emitting diodes (940 nm) were used. Screen luminance was measured with an International Light IL-1700 photometer.

## Results

### Electroretinographic identification of the nob4 mutation

We used the ERG to examine visual function in the G3 offspring in pedigrees derived from mutation-bearing G1 mice generated in an ENU mutagenesis program (Pinto *et al.*, 2004). For one pedigree we found that the ERGs of two siblings lacked a b-wave, although the a-wave and their retinal fundi appeared normal (Fig. 1 top row). The traits of both of these founders were transmitted with a recessive mode of inheritance and we generated G5 and G7 homozygous mutant mice for further studies. The scotopic threshold response (STR), a biphasic potential reflecting inner retinal activity (Saszik *et al.*, 2002) also was absent in the two G3 founder mice and each of over 30 of their progeny that also lacked the b-wave (Fig. 1 second row). The photopic ERG (background luminance 0.5 cd/m$^2$) also lacked a b-wave (Fig. 1 third row) and this absence made the a-wave appear larger compared to WT mice (Fig. 1 third row). The c-wave of *nob4* mice did not appear to be affected.

The fundoscopic appearance in *nob4* mutant mice was normal (data not shown) We examined the retinal anatomy of *nob4* retinas with H and E staining and found a normal laminar structure (Fig. 2). Thus, the mutation appeared to affect only inner retinal function. without grossly altering the retinal structure and we decided to identify the gene abnormality that was responsible for this interesting phenotype.

### Mapping and molecular cloning of the nob4 mutation

The ERG phenotype in both G3 founders was transmitted with a recessive mode of inheritance. For further studies, G5 and G7 homozygous mutant mice were generated. To

map the *nob4* mutation, *nob4* mice on a C57BL/6J (B6) background were crossed with WT DBA/2J (D2) or 129Sl/J (129) mice to produce (D2XB6)F1 or (129XB6)F1 progeny. F1 mice were intercrossed to produce (D2B6F1XB6)F2 or (129B6F1XB6)F2 mice. A total of 42 F2 mice were produced, phenotyped with the ERG, and genotyped. A nonrecombinant region was identified on chromosome 11 that contained a strong candidate gene for this phenotype, *Grm6* (encoding the mGluR6 metabolic glutamate receptor protein). Consistent with the hypothesis that *nob4*resulted from a mutation in *Grm6*, mice with null alleles for *Grm6* displayed a similar ERG phenotype (Masu *et al.*, 1995). Sequencing of the *Grm6* gene revealed a single base substitution (T709C) in codon 165 in the second exon, resulting in a predicted alteration from serine to proline. This mutation should disturb the secondary structure of the molecule in this domain and alter folding or function of the receptor.

### Grm6 mRNA expression in the retina

The levels of *Grm6* mRNA were measured in *nob4* mutant retinas, using quantitative RT-PCR. Although not significant (p=0.19, student's t-test), *Grm6* mRNA expression in *nob4* retinas was only ~60% of that in WT retinas. Consistent with our histological results, no significant changes in the expression levels of other retinal genes were observed in *nob4* retina: *rhodopsin*, *Rom1* and *Thy1* (p=0.19, 0.19, and 0.25, respectively, student's t-test).

### Immunohistochemical examination of nob4 mutant retinas

*W*e examined the pattern of mGluR6 expression in retinal sections. Figure 2 compares the patterns of expression of the rod bipolar cell marker, PKCα with mGluR6. Expression of mGluR6 could not be found in the mutant retinas although robust staining was evident in WT sections. In both *nob4* and WT mice, PKCα label showed that the dendrites, somata and axon terminals of rod bipolar cells had normal morphology and terminated in the correct retinal layers.

### Expression of mutant mGluR protein in vitro

The finding of a mutation in the Grm6 gene that leads to a predicted change from Ser to Pro in the mGluR6 receptor protein suggests, but does not prove, that this mutation is responsible for the observed phenotypes of the *nob4* mutant. To test this possibility we compared the glutamate-induced responses of mGluR6 receptor bearing the same mutation that was found in *nob4*mutan t mice with those of the appropriate WT receptors *in vitro*. Glutamate-induced currents were evoked from oocytes expressing the WT mGluR6 receptor, the Gαo-1 protein, and GIRK1-GIRK2 heterodimeric reporter ion channels (Fig. 3B) (Sharon *et al.*, 1997). However, application of glutamate to oocytes expressing the mGluR6-S165P mutant protein did not evoke detectable currents. In order to test whether the substitution of proline at the location of the mutation found in *nob4* is also deleterious in another metabotropic glutamate receptor we made similar measurements with the mGluR2 receptor. The domain structure of the mGluR2 receptor is similar to that of the mGluR6 receptor and glutamate-induced currents of oocytes expressing mGluR2 are large (Sharon *et al.*, 1997). The mGluR6-S165P mutation found in *nob4* mutant mice occurs in the middle position of a short conserved FXR sequence found in the LB1 extracellular domain of the receptor (Kunishima *et al.*, 2000). The FXR domain is found across all reported families of metabotropic glutamate receptors and we thus constructed the mGluR2-A181P mutation and expressed the mutant protein in *Xenopus* oocytes. Application of glutamate to oocytes that expressed the WT mGluR2 receptor resulted in large, Ba(II)-sensitive currents (Fig. 3A) but application of glutamate to oocytes expressing the mGluR2-A181P mutant protein did not evoke detectable currents. Western blotting of whole lysed oocytes with the appropriate antibodies that recognize intracellular epitopes demonstrated that both the WT and mutant mGluR2 and mGluR6 proteins were expressed in oocytes. It is possible either that these mutant proteins did not enter the surface membrane of the oocytes or that they entered the

surface membrane but were not functional. We did not measure surface expression levels of mGluR2 or mGluR6 in oocytes and the present work thus can not distinguish between these possibilities. The immunohistochemical studies of mutant and WT retinas failed to detect any mGluR6 protein in the mutant mice (Fig. 2), suggesting that the possibility that degradation of the mutant receptor occurs *in vivo* also needs to be considered. These results suggest that the replacement of the second residue of the conserved FXR sequence is capable of resulting in severe alterations of the characteristics of the mGluR6 receptor and is thus the probable cause of the observed retinal phenotypes.

### Single unit responses from isolated retinas in vitro

The responses to full field stimulation of single spike-generating units (predominantly RGC but including a minority of spiking amacrine cells) from the isolated retinas of *nob4* mutants differed greatly from those recorded from WT retinas in two major ways (Fig. 4). First, ON responsive units were rarely recorded in *nob4* retinas. Second, the ON response in most *nob4*ON -OFF responsive units was delayed relative to stimulus onset. One such unit is shown in Figure 4A. Interestingly, there was considerable variability in the onset of this delayed ON response (Fig. 5), suggesting that its effect on visual behavior might be minimal. To obtain an unbiased estimate of the relative contributions of ON and OFF signals in WT and *nob4* retinas, we plotted the summed high spike activity (> 1SD over the mean value) as a function of time for all *nob4*and WT cells (Fig 5). The resulting summed response shows that *nob4* retinas have no short latency ON response peak, a hallmark of WT responses to light onset. Further, the delayed ON response peak contributes minimally to the summed response.

### Single unit responses recorded in vivo from nob4 RGCs

Like the visual responses of RGCs recorded *in vitro*, *nob4* RGCs (n = 24 cells; 4 mice) recorded *in vivo* displayed significant abnormalities compared to WT cells (n = 35 cells; 6 mice). We recorded many *nob4* RGCs that were spontaneously active but not visually responsive to our full-field stimulus (12.5%; 3/24), whereas none of our WT cells were unresponsive. All of our WT RGCs could be classified as ON, OFF or ON-OFF based on the timing of their response to a full-field stimulus onset or offset (Figs 6 and 7A) and all of the ON-OFF RGCs in both WT and *nob4* were classified as OFF-center RGCs based on RF center stimulation, consistent with our previous observations (Sagdullaev & McCall, 2005; Chang *et al.*, 2006). Consistent with the *in vitro* results presented above, *nob4* ON RGCs were rarely encountered *in vivo* (17%; 4/24; Fig. 7A) while ON RGCs represented 37% of the WT population (13/35). This suggests a loss of ON RGCs in *nob4* mice (Fig. 7A). When a response to stimulus onset could be identified in *nob4* RGCs, their peak response was significantly delayed compared to WT (Fig. 7B) and the peak firing rates (Fig 7C) of these delayed *nob4* responses were significantly reduced compared to WT (26.3 + 3.3 spikes/sec vs. 73.2 + 6.5 spikes/sec; p=0.006). Together these characterizations and those *in vitro* indicate that the absence of signaling through the mGluR6 receptor results in a selective deficit in the ON pathway, a conclusion consistent with the results in the mGluR6 knockout mouse (Renteria *et al.*, 2006).

### Visually-induced behavior of nob4 mutants

The visual acuity of adult WT mice, measured using the optomotor response, is about 0.4 c/deg for photopic luminances and the peak value of the contrast sensitivity function (15–20) occurs at about 0.064 c/deg (McGill *et al.*, 2004). We found that both of these measures were severely reduced for *nob4*mice over a range of luminances from $10^{-5}$ to 58 cd/$m^2$ (Fig. 8; ANOVA, $p<<0.01$; n = 6 WT, 5 *nob4*). In fact, the entire spatial frequency tuning curve, measured with six spatial frequencies spanning a range of nearly one decade, was reduced for *nob4* mice under both scotopic and photopic conditions (Fig. 9; ANOVA, $p<<0.01$; n = 4

WT, 5*nob4* ). In contrast to the findings for WT mice, the spatial frequency tuning curve for *nob4*mutant mice did not display a clear peak, consistent with the absence of receptive field center/surround organization found in recordings *in vivo* (Fig. 6). We also measured acuity and peak contrast sensitivity at early postnatal ages (Fig. 10) and found that the behavioral deficits evident in the adult were not progressive in *nob4*mice . The deficits were apparent as early as we tested, within a day after eye opening. In both *nob4* and WT mice, some maturational improvement occurred (Fig. 10; ANOVA $p<<0.01$; n = 6 WT, 5 *nob4*), but neither acuity nor peak contrast sensitivity were ever similar to WT (Fig. 10; ANOVA $p<<0.01$; n = 6 WT, 5 *nob4*).

## Discussion

Our mapping and sequencing data suggest that the *nob4* defect results from a point mutation in the *Grm6* gene that causes a Ser to Pro substitution at residue 165 of mGluR6. Confirmation of this causal relationship comes from a number of sources. First, the absence of an ERG b-wave, when the a-wave is normal, is a phenotype consistent with a defect in signal transmission between the photoreceptors and ON bipolar cells. Second, there is a complete correlation between this genotype and the ERG phenotype in mapping crosses. Third, the retinas of *nob4*mice do not exp ress mGluR6 protein and the functional deficit is restricted to signaling through the ON pathway. Fourth, recapitulation of the mutation in both mGluR6 and the related mGluR2 receptor *in vitro* produces a defective protein (Fig 3). Finally, the phenotype is similar both to that described in the *mGlur6* knockout mouse and in humans with autosomal recessive congenital stationary night blindness (arCSNB) resulting from a mutation in the *GRM6* gene (Dryja *et al.*, 2005; Zeitz *et al.*, 2005; O'Connor *et al.*, 2006). Thus, the conclusion that the identified mutation in *Grm6* is responsible for the observed *nob 4* visual phenotypes is well-supported.

Defects in visual processing were found at three different levels in *nob4*mice und er both scotopic and photopic conditions: the depolarizing bipolar cell, the RGC, and behaviorally. Specfically, *nob4* mice lack an ERG b-wave, while the a-wave is spared. This implies that although the photoreceptors hyperpolarize in response to a light stimulus, transmission to second order retinal neurons, in particular the depolarizing (rod and On cone) bipolar cells (Sharma et al, 2005), is compromised. The absence of the STR of *nob4* ERGs suggests that transmission also is reduced between bipolar cells and their postsynaptic partners (Saszik *et al.*, 2002).

The defects in the visual responses of *nob4* RGCs support this conclusion and demonstrate that the defect is specific to the ON pathway. The majority of *nob4* RGCs recorded both *in vitro* and *in vivo* only respond to the offset of a light stimulus. In addition, there is a concomitant increase in the percentage of RGCs with spontaneous but no visually-evoked activity in *nob4* mice. When *nob4*RGCs with a response to light onset were found, the responses were abnormal. First, the ON response was significantly delayed, relative to the stimulus onset and the timing of the onset of the response was variable. Further, ON responses contributed little to the overall response of the retina, as their excitatory responses were very small. These observations also are consistent with defects observed in RGCs in *Grm6* null mice (Renteria *et al.*, 2006) and with the absence of ON responses in both the superior colliculus (Masu *et al.*, 1995) and visual cortex (Renteria *et al.*, 2006) of *Grm6* null mice. Thus, a point mutation in the *Grm6* gene is capable of disrupting gene function, similar to that produced by a null allele. In contrast to the ON responses, the OFF responses of *nob4*RGCs appear unaffected, a result consistent with the conclusion that the ON and OFF pathways are separate and that the OFF pathway carries a delayed ON response, observed in ON-OFF responsive single units.

It is interesting to note that, although the ON and OFF pathways are thought to be parallel and separate, our behavioral data argue that normal function in both pathways are required to interpret spatial patterns of light and dark that comprise our visual environment. The absence of one pathway in *nob4* mice results in severe deficits in both visual acuity and contrast sensitivity at both photopic and scotopic conditions. This decrease in visual performance is so pronounced that the spatial frequency tuning curves of *nob4* mice fail to display a clear peak. When visual behavior of either *nob* (Gregg *et al.*, 2003) or *Grm6* null (Masu *et al.*, 1995) mutant mice were assayed, using a shuttle box avoidance task with a full-field light stimulus as the cue, their learning curves were similar to WT. However, when the luminance of this cue was decreased performance in *nob* mice dropped quickly (Gregg *et al.*, 2003).

Similarly, our comprehensive assay of spatial vision clearly shows that some vision is mediated through the OFF pathway in *nob4* mice. However, information only through this pathway is insufficient for normal levels of pattern vision, whereas it is probably sufficient for simple luminance detection.

Our data do not address why the mutation from Ser to Pro at position 165 of *Grm6* reduces expression of the mGluR6 protein to undetectable levels. However, examination of the crystallographic structure of the related mGluR1 protein (Kunishima *et al.*, 2000) shows that the S165P mutation lies in a β sheet that adjoins a helix containing a ligand-interacting Asp residue (D191 of mGluR6) and a β sheet containing a ligand-interacting Thr residue (T185) (Rosemond *et al.*, 2004). Perhaps substitution of the proline residue in the mutant protein results in misfolding of the protein and degradation prior to insertion into the plasma membrane. Mutations in both the mGluR6 receptor and the related mGluR2 receptor produced *in vitro* resulted in a defective protein (Fig 3).

The elucidation of mechanisms underlying important biological processes is aided by the availability of two sets of mutations; an allelic series of mutations that affect a given gene product involved in the process as well as a series of mutations that affect each of several gene products involved in the process. Thus, studies of the mechanism and role of the ON pathway in the visual system will be expedited by the availability of mutations that affect various gene products in this pathway. Together with *nob4* allele (mGluR6 -S165P), mutations in nyctalopin (*nob* mutation) (Pardue *et al.*, 1998; Gregg *et al.*, 2003), a voltage-gated calcium channel (*Cacna1f* gene, *nob2* mutation) (Chang *et al.*, 2006) and the knockout of mGluR6 (Masu *et al.*, 1995), should be of great help in the study of the function of the essential ON pathway. Mutant mice can be obtained at cost by academic investigators at http://www.neuromice.org/.

## Acknowledgments

Supported by NIH Cooperative Research Agreement U01MH61915, R01 EY06669 (JBT), R01 EY014701 (MAMc). DRC was supported by the National Defense Science and Engineering Graduate Fellowship and SI was supported by the US Fulbright Program.

## References

Chang B, Heckenlively JR, Bayley PR, Brecha NC, Davisson MT, Hawes NL, Hirano AA, Hurd RE, Ikeda A, Johnson BA, McCall MA, Morgans CW, Nusinowitz S, Peachey NS, Rice DS, Vessey KA, Gregg RG. The nob2 mouse, a null mutation in Cacna1f: anatomical and functionalabnormalities in the outer retina and their consequences on ganglion cell visual responses. Vis Neurosci. 2006; 23:11–24. [PubMed: 16597347]

Dawson WW, Trick GL, Litzkow CA. Improved electrode for electroretinography. Invest Ophthalmol Vis Sci. 1979; 18:988–991. [PubMed: 478786]

Dryja TP, McGee TL, Berson EL, Fishman GA, Sandberg MA, Alexander KR, Derlacki DJ, Rajagopalan AS. Night blindness and abnormal cone electroretinogram ON responses in patients with mutations in the GRM6 gene encoding mGluR6. Proc Natl Acad Sci U S A. 2005; 102:4884–4889. [PubMed: 15781871]

Gregg RG, Mukhopadhyay S, Candille SI, Ball SL, Pardue MT, McCall MA, Peachey NS. Identification of the gene and the mutation responsible for the mouse nob phenotype. Invest Ophthalmol Vis Sci. 2003; 44:378–384. [PubMed: 12506099]

Kuffler SW. Discharge patterns and functional organization of mammalian retina. J Neurophysiol. 1953; 16:37–68. [PubMed: 13035466]

Kunishima N, Shimada Y, Tsuji Y, Sato T, Yamamoto M, Kumasaka T, Nakanishi S, Jingami H, Morikawa K. Structural basis of glutamate recognition by a dimeric metabotropicglutamate receptor. Nature. 2000; 407:971–977. [PubMed: 11069170]

Masu M, Iwakabe H, Tagawa Y, Miyoshi T, Yamashita M, Fukuda Y, Sasaki H, Hiroi K, Nakamura Y, Shigemoto R, et al. Specific deficit of the ON response in visual transmission bytargeted disruption of the mGluR6 gene. Cell. 1995; 80:757–765. [PubMed: 7889569]

McGill TJ, Douglas RM, Lund RD, Prusky GT. Quantification of spatial vision in the RoyalCollege of Surgeons rat. Invest Ophthalmol Vis Sci. 2004; 45:932–936. [PubMed: 14985313]

Morgans CW, Bayley PR, Oesch NW, Ren G, Akileswaran L, Taylor WR. Photoreceptorcalcium channels: insight from night blindness. Vis Neurosci. 2005; 22:561–568. [PubMed: 16332266]

Morgans CW, Ren G, Akileswaran L. Localization of nyctalopin in the mammalian retina. Eur J Neurosci. 2006; 23:1163–1171. [PubMed: 16553780]

Nirenberg S, Carcieri SM, Jacobs AL, Latham PE. Retinal ganglion cells act largely asindependent encoders. Nature. 2001; 411:698–701. [PubMed: 11395773]

Nirenberg S, Meister M. The light response of retinal ganglion cells is truncated by a displaced amacrine circuit. Neuron. 1997; 18:637–650. [PubMed: 9136772]

O'Connor E, Allen LE, Bradshaw K, Boylan J, Moore AT, Trump D. Congenital stationarynight blindness associated with mutations in GRM6 encoding glutamate receptor MGluR6. Br J Ophthalmol. 2006; 90:653–654. [PubMed: 16622103]

Pardue MT, McCall MA, LaVail MM, Gregg RG, Peachey NS. A naturally occurring mousemodel of X-linked congenital stationary night blindness. Invest Ophthalmol Vis Sci. 1998; 39:2443–2449. [PubMed: 9804152]

Pinto LH, Vitaterna MH, Shimomura K, Siepka SM, McDearmon EL, Fenner D, Lumayag SL, Omura C, Andrews AW, Baker M, Invergo BM, Olvera MA, Heffron E, Mullins RF, Sheffield VC, Stone EM, Takahashi JS. Generation, characterization, and molecular cloning of the Noerg-1 mutation of rhodopsin in the mouse. Vis Neurosci. 2005; 22:619–629. [PubMed: 16332273]

Pinto LH, Vitaterna MH, Siepka SM, Shimomura K, Lumayag S, Baker M, Fenner D, Mullins RF, Sheffield VC, Stone EM, Heffron E, Takahashi JS. Results from screening over 9000 mutation-bearing mice for defects in the electroretinogram and appearance of the fundus. Vision Res. 2004; 44:3335–3345. [PubMed: 15536001]

Renteria RC, Tian N, Cang J, Nakanishi S, Stryker M, Copenhagen M. Intrinsic ON responsesof the retinal OFF pathway are suppressed by the ON pathway. J Neurosci. 2006 in press.

Rosemond E, Wang M, Yao Y, Storjohann L, Stormann T, Johnson EC, Hampson DR. Molecular basis for the differential agonist affinities of group III metabotropic glutamate receptors. Mol Pharmacol. 2004; 66:834–842. [PubMed: 15231870]

Sagdullaev BT, McCall MA. Stimulus size and intensity alter fundamental receptive-field properties of mouse retinal ganglion cells in vivo. Vis Neurosci. 2005; 22:649–659. [PubMed: 16332276]

Saszik SM, Robson JG, Frishman LJ. The scotopic threshold response of the dark-adapted electroretinogram of the mouse. J Physiol. 2002; 543:899–916. [PubMed: 12231647]

Sharon D, Vorobiov D, Dascal N. Positive and negative coupling of the metabotropic glutamatereceptors to a G protein-activated K+ channel, GIRK, in Xenopus oocytes. J Gen Physiol. 1997; 109:477–490. [PubMed: 9101406]

Shimbo K, Brassard DL, Lamb RA, Pinto LH. Ion selectivity and activation of the M2 ion channel of influenza virus. Biophys J. 1996; 70:1335–1346. [PubMed: 8785289]

Siepka SM, Takahashi JS. Forward genetic screen to identify circadian rhythm mutants in mice. Methods in Enzymology. 2005; 393:217–228.

Slaughter MM, Miller RF. 2-amino-4-phosphonobutyric acid: a new pharmacological tool forretina research. Science. 1981; 211:182–185. [PubMed: 6255566]

Stern-Bach Y, Bettler B, Hartley M, Sheppard PO, O'Hara PJ, Heinemann SF. Agonistselectivity of glutamate receptors is specified by two domains structurally related to bacterialamino acid-binding proteins. Neuron. 1994; 13:1345–1357. [PubMed: 7527641]

Vitaterna MH, Pinto LH, Takahashi JS. Large-scale mutagenesis and phenotypic screens for thenervous system and behavior in mice. Trends Neurosci. 2006; 29:233–240. [PubMed: 16519954]

Zeitz C, van Genderen M, Neidhardt J, Luhmann UF, Hoeben F, Forster U, Wycisk K, Matyas G, Hoyng CB, Riemslag F, Meire F, Cremers FP, Berger W. Mutations in GRM6 cause autosomalrecessive congenital stationary night blindness with a distinctive scotopic 15-Hz flickerelectroretinogram. Invest Ophthalmol Vis Sci. 2005; 46:4328–4335. [PubMed: 16249515]

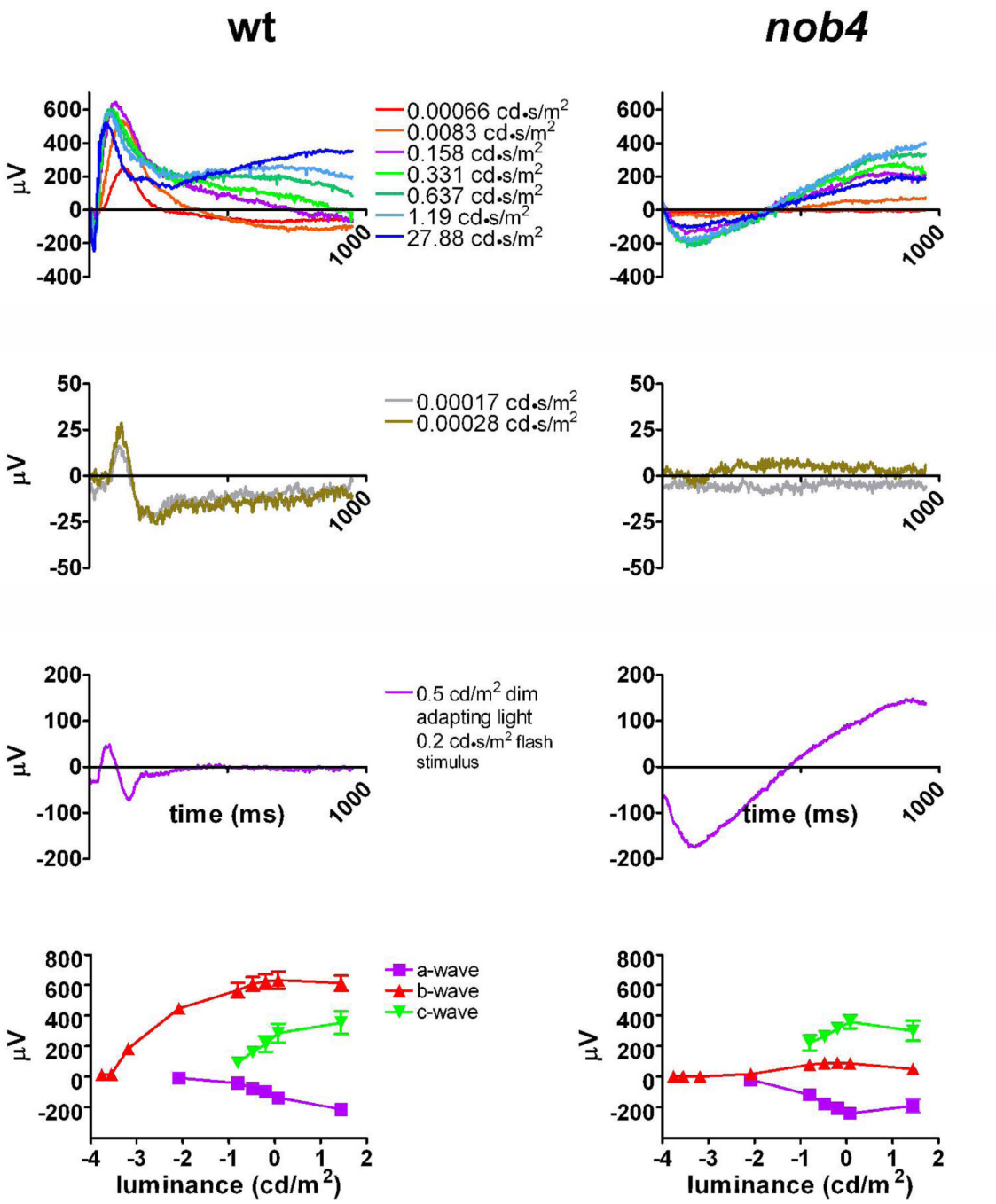


**Figure 1.**

A. Electroretinograms of wild-type (WT) (left) and *nob4* mutant (right) mice. The numbers between the traces give the energy of the flash stimuli that were used. Upper traces show the rod ERG; the second row of traces shows the scotopic threshold response (STR), and the third row of traces shows the light-adapted (0.5 cd/m$^2$) ERG. The lower graphs plot the peak values (mean + SEM; 6 mice of each genotype) for the dark adapted responses against stimulus energy. Note that the b-wave and STR of the ERG were absent from the mutant (upper and second rows) and that lack of b-wave from the light-adapted mutant ERG causes the a-wave to appear larger (third row).

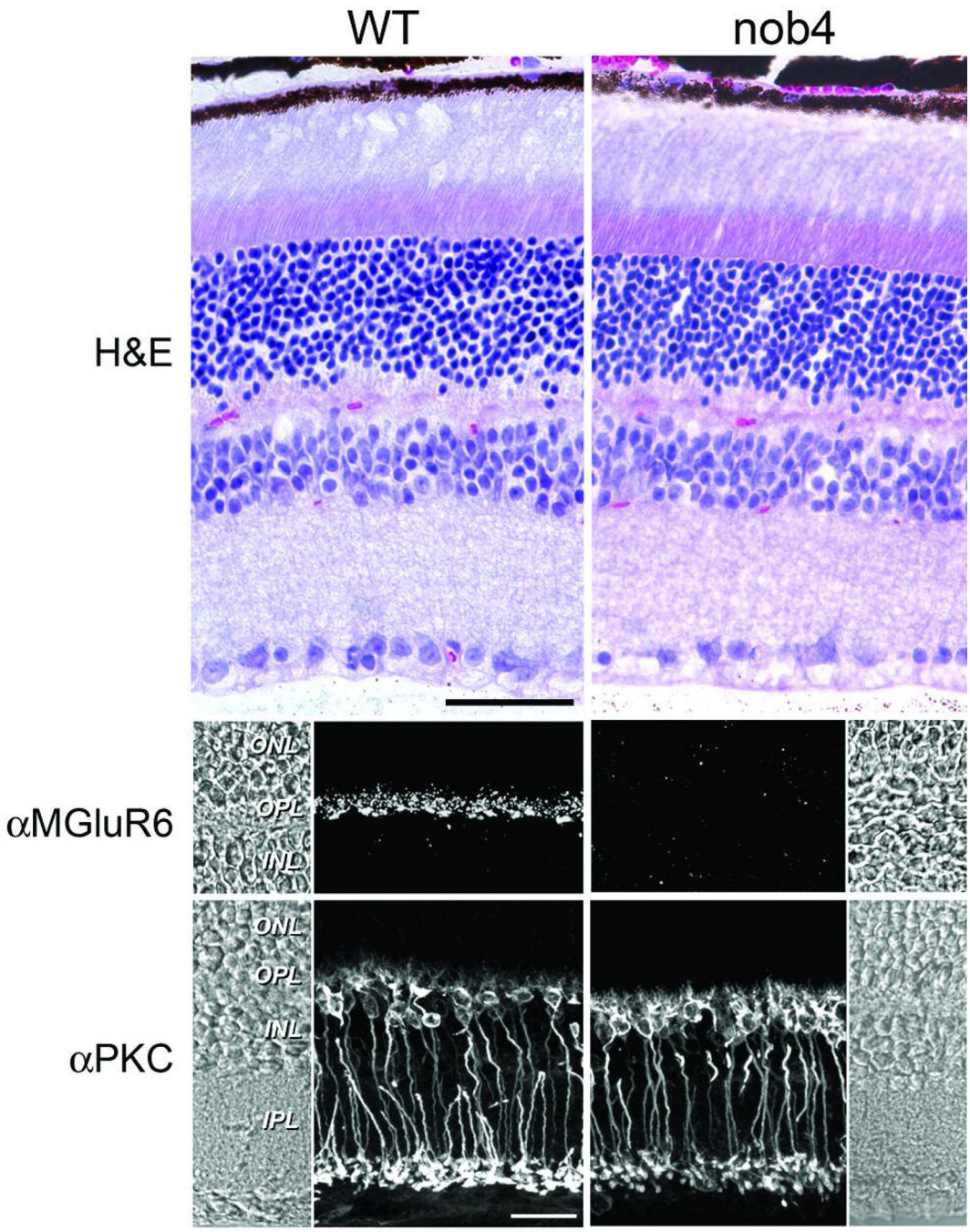


**Figure 2.**

Histological appearance of the *nob4* retina compared with that of the wild-type (WT) retina (upper) and immunofluorescent localization of mGluR6 and PKCα in the *nob4* and WT retina (lower). Mouse retina sections labeled by immunofluorescence with antibodies against either mGluR6 or PKCα revealed that the nob4 retina contains no mGluR6 immunoreactivity. Rod-BPCs of *nob4* mutants have largely normal morphology as indicated by the PKCα labeling, though the subcellular distribution of PKCα appears somewhat altered. Scale bar represents 20 mm and applies to all panels. Abbreviations are as follows: OS, outer segments; IS, inner segments; ONL, outer nuclear layer; OPL, outer plexiform layer; INL, inner nuclear layer; IPL, inner plexiform layer.

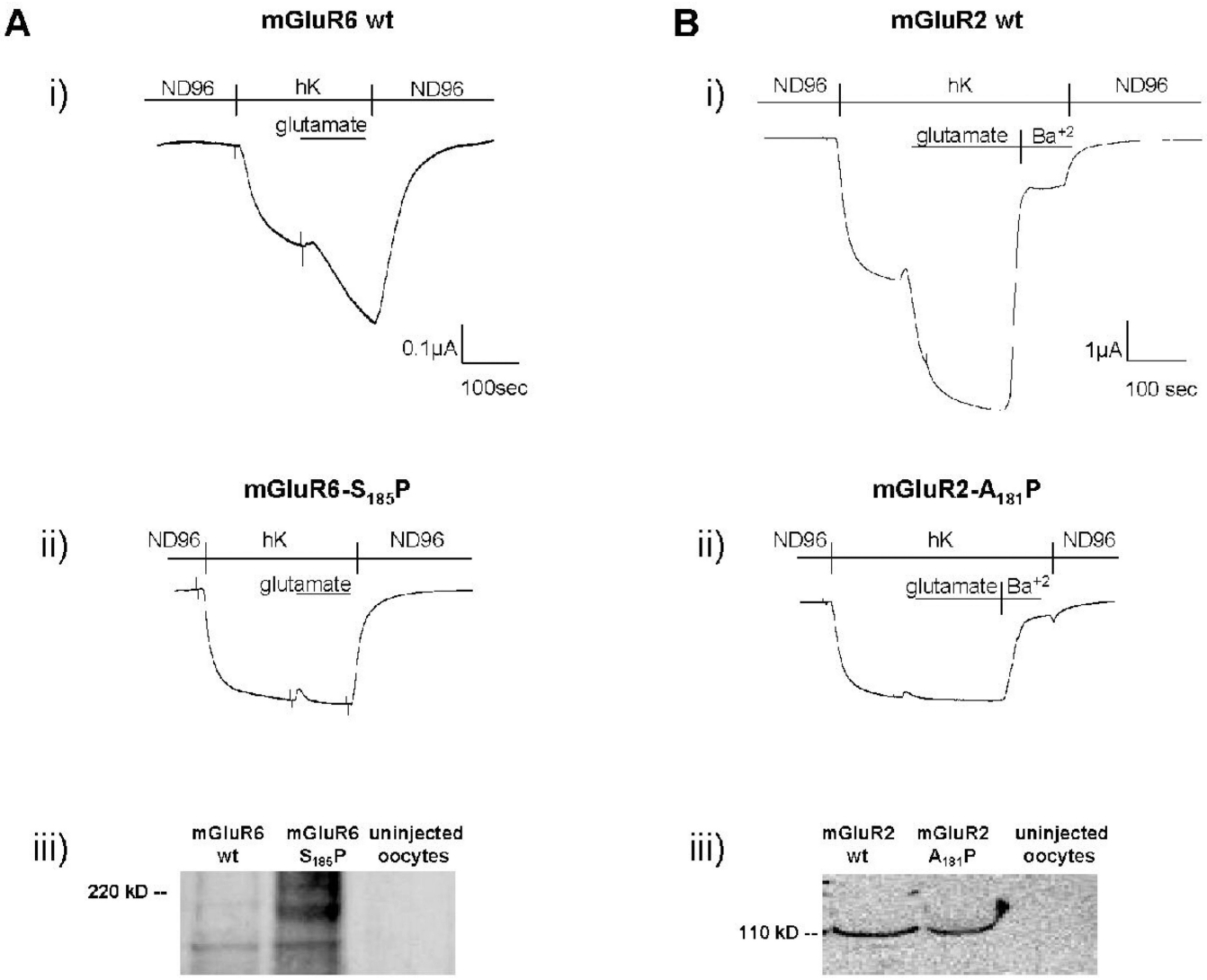


**Figure 3.**

*In vitro* expression of mGluR6 and mGluR2 WT and mutant receptors in *Xenopus* oocytes. Oocytes also expressed GIRK1 and GIRK2 ion channels as reporters of activation of the receptors and, in experiments with mGluR6, Gαo-1was co-expressed. Large inward currents flow through GIRK channels when the expressing cell is exposed to elevated $K^+$ (hK), and activation of mGluR2 or mGluR6 by glutamate increases the GIRK currents. **A**. Two-electrode voltage-clamp recording from oocytes expressing the (i) mGluR6 wild type and (ii) mGluR6-S185P mutant receptor. Bars above traces show solution applied. (iii). Western blot analysis on whole-cell protein fractions (obtained from 14 oocytes) was performed as described in Methods. **B**. Two-electrode voltage-clamp recording from oocytes expressing the (i) mGluR2 wild type and (ii) mGluR2-A181P mutant receptor. Bars above traces show solution applied. (iii). Western blot analysis on whole-cell protein fractions (obtained from 10 oocytes) was performed as described in Methods. Note that the mutant proteins were expressed in oocytes but that application of the activator (glutamate) did not result in an increase in current through the GIRK reporter ion channel.

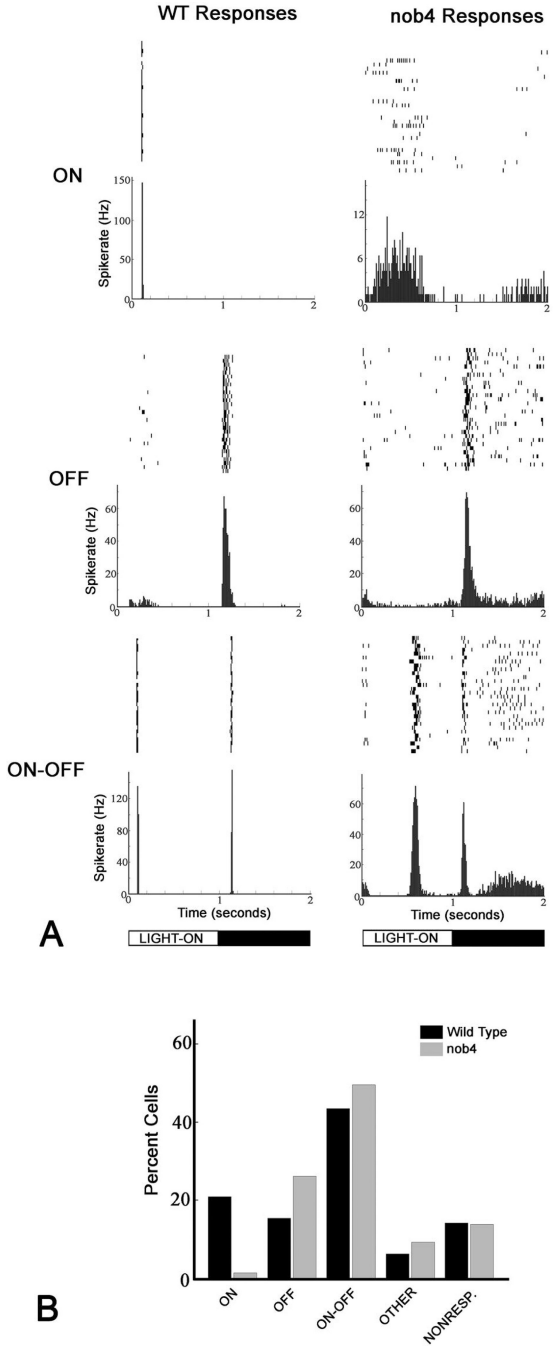


**Fig. 4.**

A. Representative spike raster plots and peristimulus time histograms (PSTH, binwidth 10 ms) of ON, OFF and ON-OFF cell responses recorded from *in vitro* WT and *nob4* retinas. Note the delayed ON response for the ON-OFF cell of the *nob4* mouse. All responses were evoked by a full field flash visual stimulus, whose timecourse (1 s light ON and 1 s light OFF) is shown at the base of the figure. B. Percentages of cell classes for wild type and *nob4* mutant mice, based on recordings from 163 cells from two wild type retinas and 153 cells from two *nob4* mutant retinas.

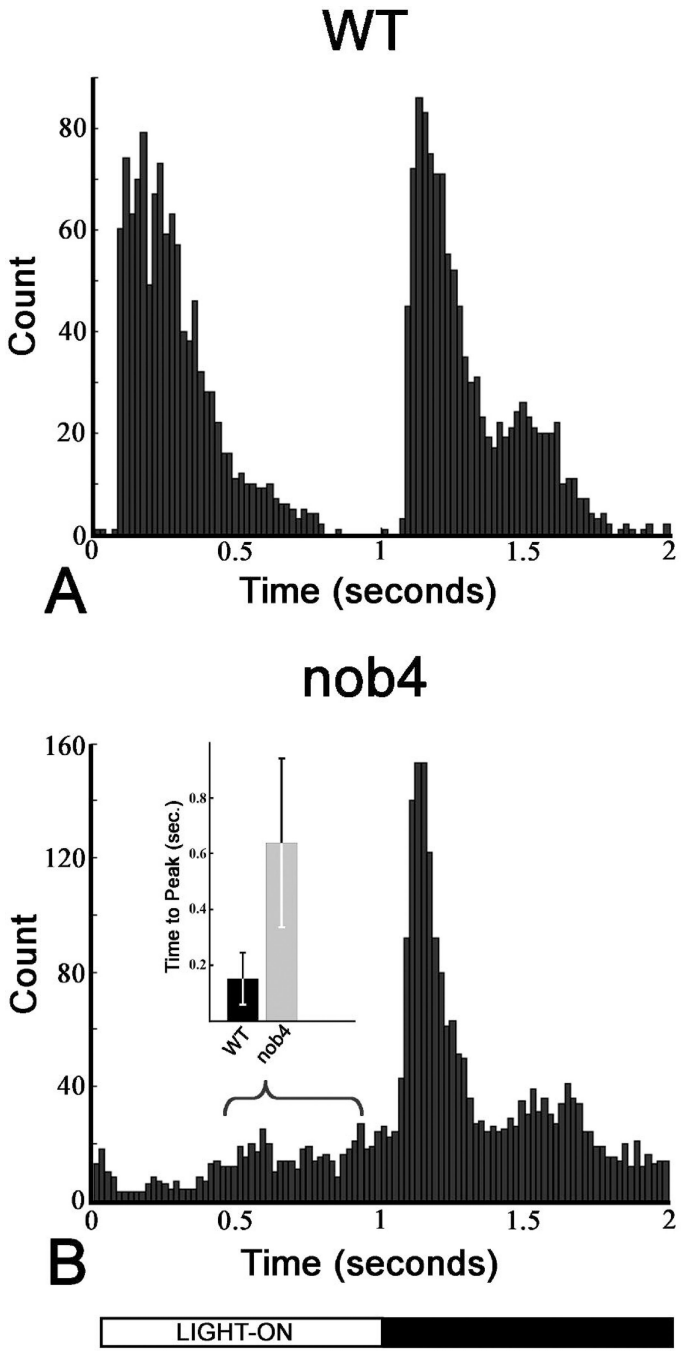


**Fig. 5.**

High spike activity time course histograms for WT and *nob4* mutant mice *in vitro*. Histograms of high spike activity as a function of stimulus time were generated by counting, from every cell (ON, OFF, ON-OFF, Nonresponsive and Other), the times at which the spike rate was greater than one standard deviation above the mean spike rate of the cell. These histograms measure the time-course of high spike activity within the population of RGCs. The wild type histogram (A) displays peaks during both the ON and OFF portions of the light stimulus. The *nob4* histogram (B), however, displays a peak during only the OFF portion of the stimulus. The dispersion in the time of the delayed ON response is indicated by the bracket shown in B, which spans the lower and upper quartiles of this response. The

inset shows for WT and *nob4* the means and standard deviations of the latency of the ON responses of ON-OFF cells.

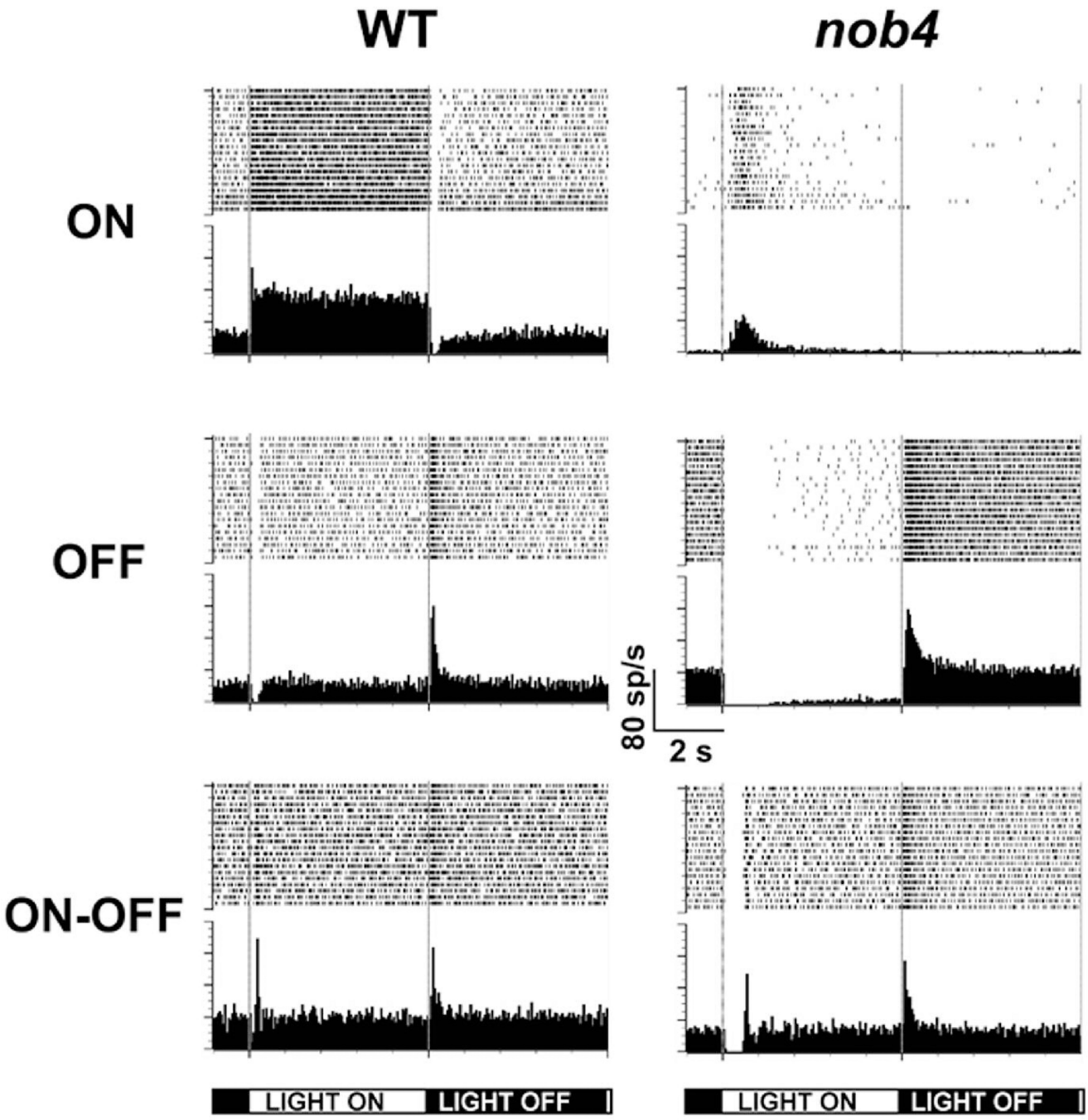


**Figure 6.**

Raster plots and average post-stimulus time histograms of typical wild-type (WT) and *nob4* retinal ganglion cell (RGC) responses to full field stimuli recorded from mice *in vivo*. Individual RGC responses were isolated from the optic nerve of mice *in vivo* and the receptive field location determined. RGCs were stimulated with a full field stimulus of 5 sec light ON (150 cd/m$^2$) and 5 sec light OFF (0 cd/m$^2$). Typical responses for single WT (left panel) and *nob4* (right panel) RGCs are plotted as raster plots and average post-stimulus time histograms (50 ms bin width). Based on their responses to full field stimuli, RGCs could be classified as ON-(top), OFF-(middle) or ON-OFF (bottom). In addition, a subset of the *nob4* RGCs was unresponsive (not shown).

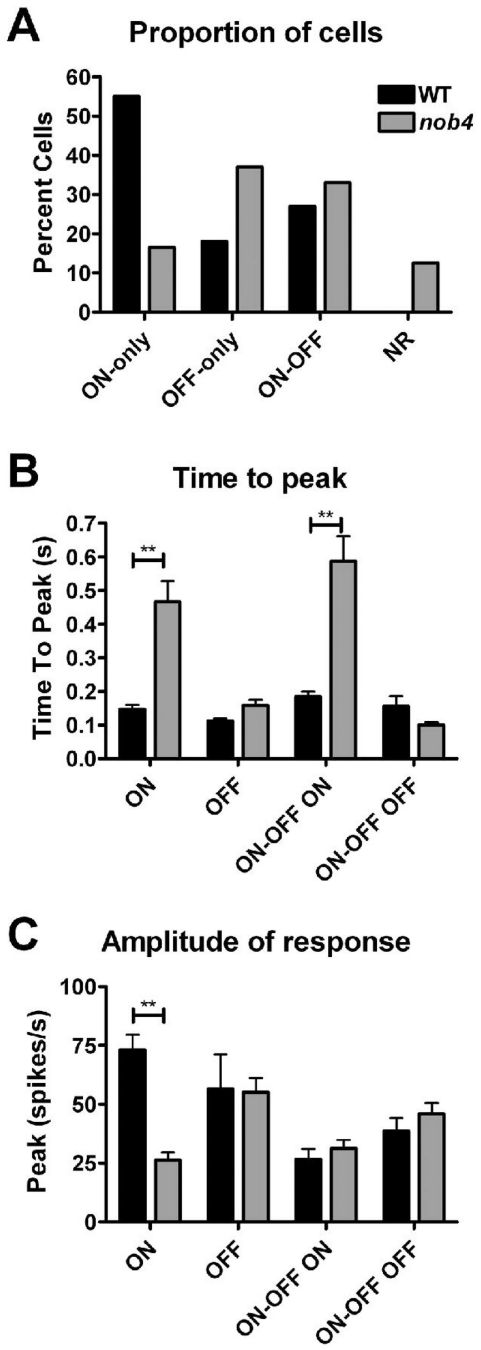


**Figure 7.**

The proportions, kinetics and amplitudes of retinal ganglion cell (RGC) responses recorded from wildtype (WT) and *nob4*mice *in vivo*. Individual RGC responses were isolated from the optic nerve of mice *in vivo* and characterized based on their response to a full field stimulus of 5 sec light ON (150 cd/m$^2$) and 5 sec light OFF (0 cd/m$^2$). Cells could be classified as ON (n=22 WT, n=4 *nob4*), OFF (n=5 WT, n=9 *nob4*), ON-OFF (n=8 WT, n=8 *nob4*) or unresponsive (n=0 WT, n=3 *nob4*). A) The proportion of each cell class recorded from WT and *nob4* mice presented as a percentage of the total cell number. B) The time to peak and C) the peak amplitude of the excitatory response of RGCs from WT and *nob4*mice plotted as a function of cell class, where ON was obtained from the response of ON only

RGCs; OFF was obtained from OFF-only RGCs; ON -OFF ON and ON-OFF OFF were obtained from the ON and OFF excitatory responses respectively, recorded from ON-OFF cells.

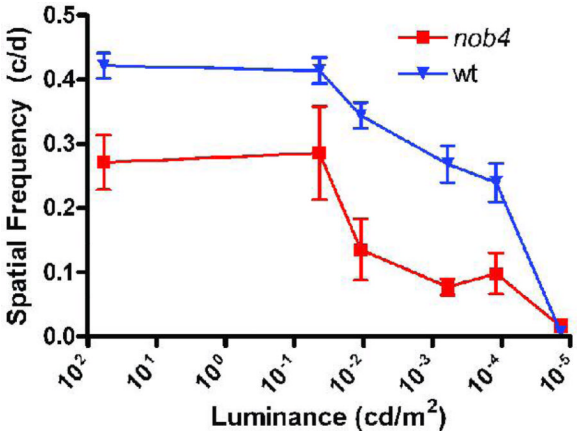


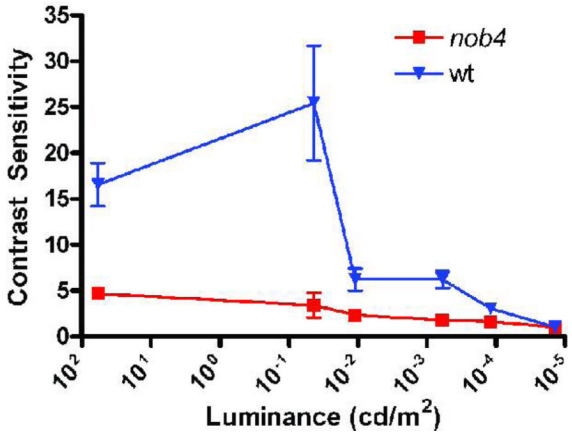


**Figure 8.**

Comparison of visual acuity (left) and peak contrast sensitivity (right; measured at 0.064 c/deg) for WT and *nob4* mutant mice as a function of luminance. Both of these measures of visual function were made using optomotor responses and were decreased in the mutant retinas for every value of luminance tested above $10^{-5}$ cd/m$^2$, at which luminance the responses became unreliable.

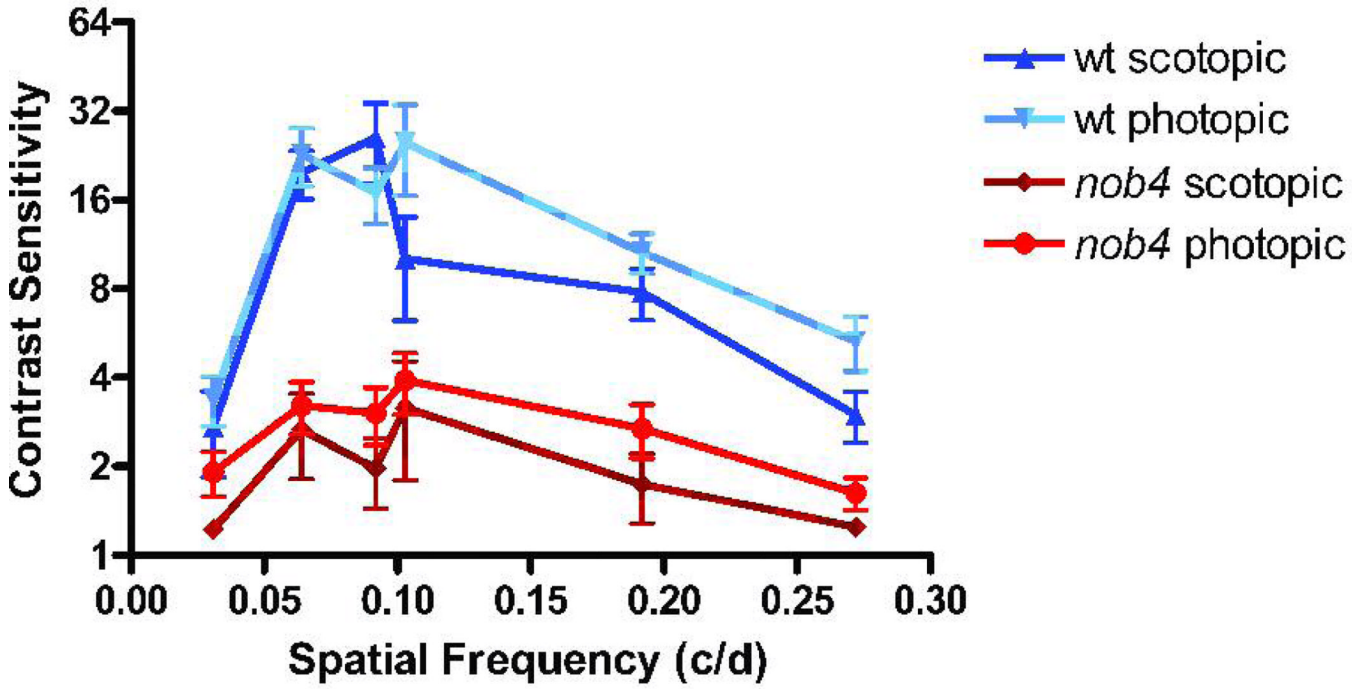


**Figure 9.**

Comparison of the spatial frequency tuning curves of WT and *nob4*mutant mice. Note that the contrast sensitivity function, measured under both scotopic and photopic conditions, had a clear peak for the WT mice but did not have a peak for the mutant mice and that the values for the mutant mice were lower for all spatial frequencies.

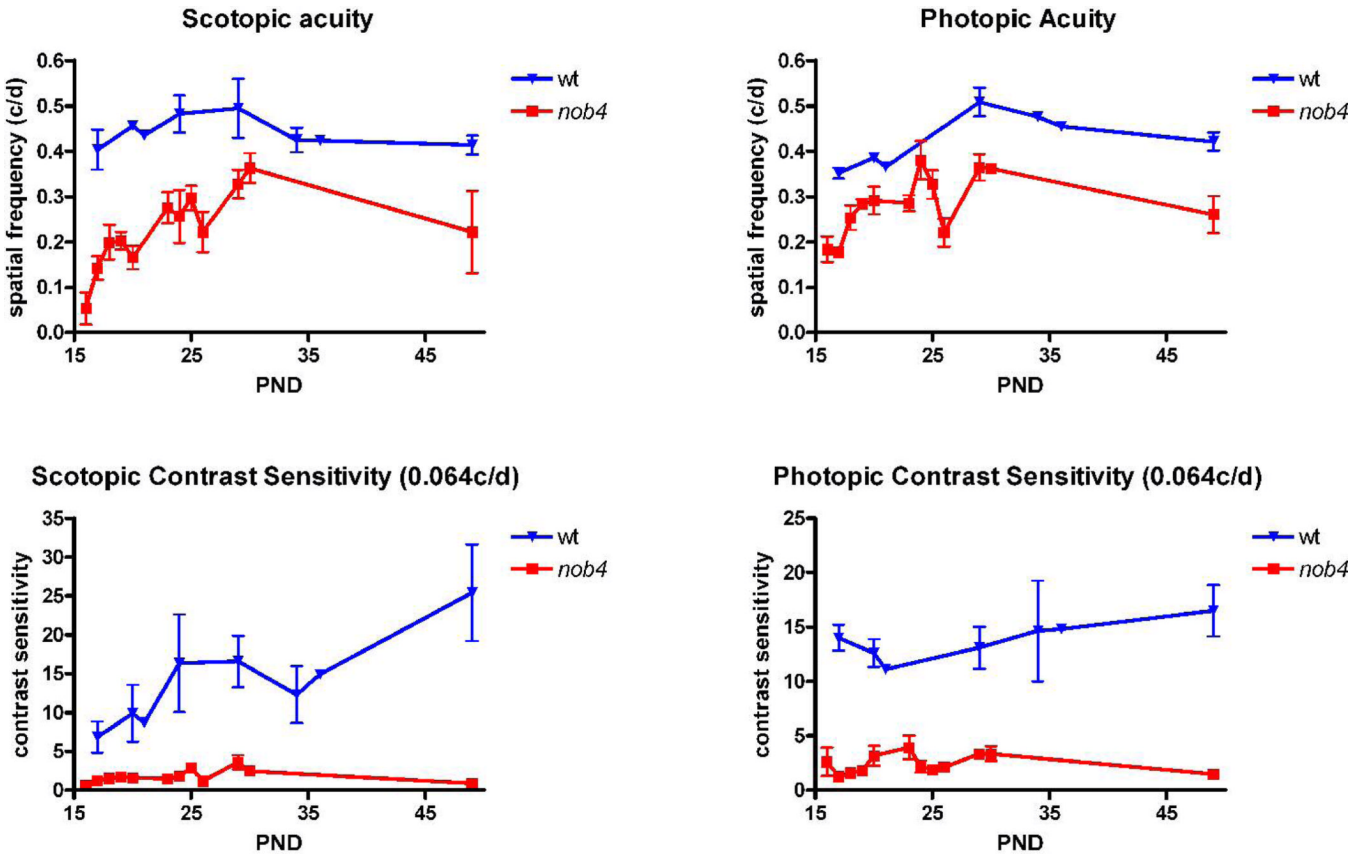


**Figure 10.**

Comparison of the time course of development of acuity (upper panels) and peak contrast sensitivity (0.064 c/deg, lower panels) of WT and *nob4* mutant mice. These variables were measured from shortly after eye opening until PND 49 for both photopic (left panels, 58.5 cd/m$^2$) and scotopic (right panels, 3.2 $10^{-2}$ cd/m$^2$) luminances. Note that the mutants did not attain the same values of acuity or contrast sensitivity that are attained by WT mice.